Near-ice Hydrographic Data from Seaglider Missions in the Western Greenland Sea in Summer 2014 and 2015

Katrin Latarius[1], Ursula Schauer[2], Andreas Wisotzki[2]

[1]Bundesamt für Seeschifffahrt und Hydrographie (Federal Marine and Hydrographic Agency), 20359 Hamburg, Germany
[2]Alfred Wegener Institute, Helmholtz Centre for Polar and Marine research, 27570 Bremerhaven, Germany

Correspondence to: Katrin Latarius (katrin.lataroius@bsh.de)

Abstract. During summer 2014 and summer 2015 two autonomous Seagliders were operated over several months close to the ice edge of the East Greenland Current to capture the near-surface fresh water distribution in the western Greenland Sea. The mission 2015 included an excursion onto the East Greenland Shelf into the Norske Trough. Temperature, salinity and drift data were obtained in the upper 500 to 1000 m with high spatial resolution.

At AWI the data processing for these glider measurements was conducted. The first part consists of the Seaglider Toolbox from the University of Each Anglia, the second was exclusively composed for the data from the Greenland Sea.

The final hydrographic, position and drift data sets can be downloaded from
https://doi.org/10.1594/PANGAEA.893896.

1   Introduction

The Nordic Seas are shaped by a strong near-surface salinity contrast arising from the northward flow of saline Atlantic Water along their eastern rim and the southward flow of fresh Polar Water and sea ice along their western rim in the East Greenland Current (EGC) (Fig. 1). Due to strong cooling in winter, the Nordic Seas are one of the few regions in the World Ocean where convection normally reaches depths of 500 to 2000 m (Nansen,

35   1906; Rudels et al., 1989; Budéus and Ronski, 2009). With this intermediate water ventilation it contributes substantially to the Atlantic Overturning Circulation (Schmitz and McCartney, 1993; Lumpkin and Speer, 2003). The convective overturning depends on the density stratification, which in the cold Nordic Seas is mostly set through salinity.
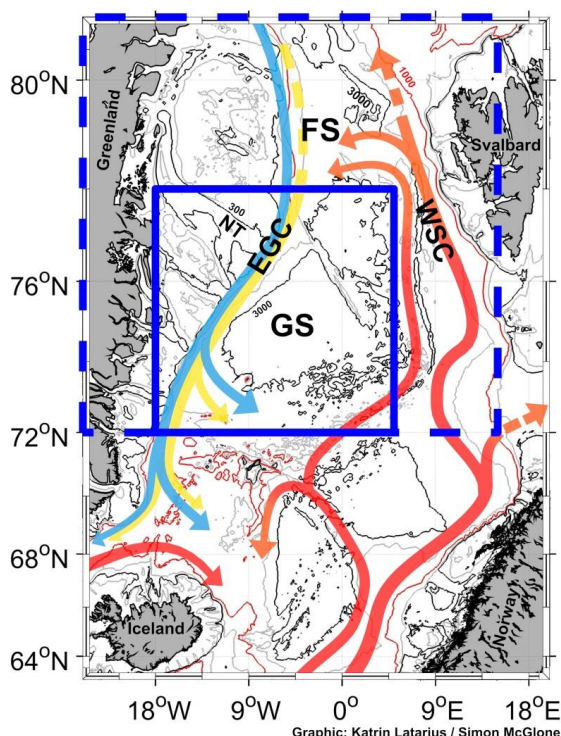
40

Figure 1: The map shows the Nordic Seas. Topographic contours are given on the basis of RTOPO2 (Schaffer et al., 2016): the 1000 m contour is marked in red, the 3000 m and 300 m contours in black, and the 2000 m, 500 m and 200 m contours in gray. The inlet marked by the full blue line shows the area of
45   **Fig. 2, the inlet marked by the dashed blue line shows the area of Fig. 3.**
EGC – East Greenland Current, WSC – West Spitsbergen Current, FS – Fram Strait, GS – Greenland Sea, NT – Norske Trough.
Red to yellow arrows indicate the flow of warm and saline Atlantic Water; and the cooling on the way through the Nordic Seas and Arctic Ocean. The blue arrows indicate the flow of cold and fresh Polar
50   **Water through the Nordic Seas.**

The EGC transports between 50 % and 75 % of the liquid freshwater and sea ice output from the Arctic Ocean through the Nordic Seas to the subpolar North Atlantic (Aagaard and Carmarck, 1989; Serreze et al., 2006). More freshwater is added to the current by the runoff from Greenland (Bamber et al., 2012). The transport of

55   freshwater in the EGC both liquid and frozen varies on interannual to decadal time scales (Smedsrud et al., 2011; Hansen et al., 2013; Spreen et al., 2009).

During late summer, frequently low salinities were observed in the near-surface layer of the deep basin of the Greenland Sea (GS) (Latarius and Quadfasel, 2016). However, this seasonal signal shows large inter-annual
60   variability in magnitude and vertical extension. A fresh surface layer stabilizes the water column and may reduce wintertime convection in the GS (Latarius and Quadfasel, 2016). Oltmanns et al. (2018) observed the effect of slashed convection by a fresh surface layer for the Irminger Sea in winter 2010/2011. Very likely, the freshwater in the inner western Nordic Seas originates from the EGC, yet the explicit sources as well as the transport mechanisms are still unclear. De Steur et al. (2015) revealed local ice melt as the primary source for freshwater
65   in the GS for summers 2011 and 2013. Dodd et al. (2009) found that a significant amount of sea ice leaves the EGC into the Nordic Seas whereas the liquid freshwater remains in the EGC up to Denmark Strait. However, possibly also liquid freshwater from the EGC may reach the inner western Nordic Sea. The transfer to the interior Nordic Seas may take place by eddies shedding off the Polar Front (Spall, 2011; Lherminier et al., 1999).

70   To investigate the spreading of freshwater from the western rim into the convection regions of the inner Nordic Seas, the project "Variation of freshwater in the western Nordic Seas" was conducted in the framework of the Research Group FOR1740: "A new approach toward improved estimates of Atlantic Ocean freshwater budgets and transports as part of the global hydrological cycle", funded by the German Research Association (DFG). The goal of this project is to capture and analyze fluctuations of freshwater in the western Nordic Seas and
75   understand related processes. To achieve the necessary observations over several months with high spatial resolution two missions were conducted in the summer months of 2014 and 2015 in the western GS using autonomous gliders (Fig. 2). The gliders were operated in ice-free regions, but close to the ice edge. As glider navigation in shallow waters is difficult, the sections were limited to areas with water depth greater than 300 m.
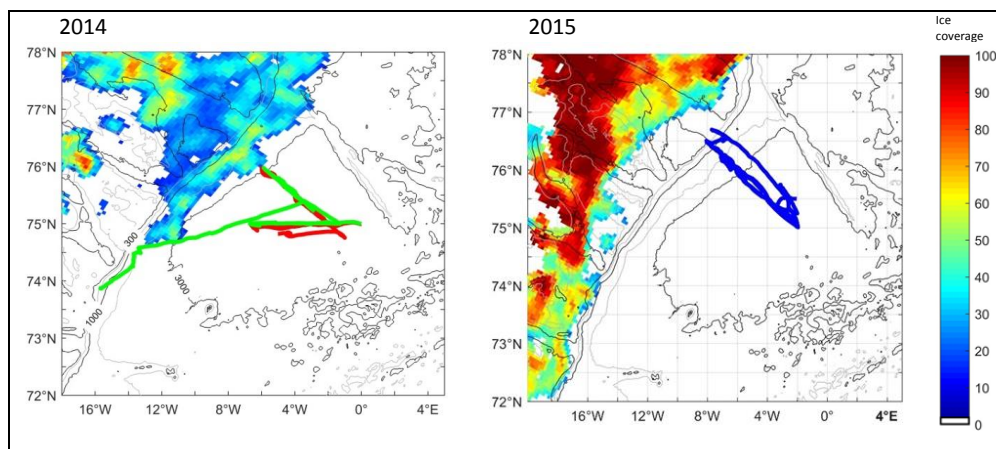
80
Figure 2: Maps of the Seaglider missions in 2014 and 2015.
2014 (left): the thick red line shows the track of Seaglider 127 and the thick green line the track of Seaglider 558.
2015 (right): the thick blue line shows the track of Seaglider 127.

85 **The thin black lines give water depth contours of 300 m, 1000 m and 3000 m as annotated for 2014 and the thin gray lines depth contours of 200 m, 500 m and 2000 m (not annotated) based on RTOPO2 (Schaffer et al., 2016). The color-coding denotes the concentration of sea ice in percent as derived from the sea ice data made available by DRIFT&NOISE (driftnoise.com); left: 2014/08/14, right: 2015/08/01. Details of the missions are summarized in Table 1. The development of the ice coverage during the missions time is**
90 **described in detail in Section 2.4.**

In this paper we describe the details of the two missions in the challenging region near the ice edge and the shallow shelf east of Greenland (Section 2), the processing of the data and appendant uncertainties and error estimates (Section 3). In the last section, we give a brief description of the observations.

95

The hydrographic and drift data of both glider missions were published in the World Data Center PANGAEA.

2 Seaglider Mission 2014 and 2015 in the western Greenland Sea

100

2.1 The western Greenland Sea

The glider missions in summer 2014 and 2015 took place in the GS, which is the northernmost basin of the
Nordic Seas (Fig. 1). The GS basin is up to 3600 m deep and flanked to the west by the steep continental slope
105   east of Greenland. The EGC is flowing along the shelf break and the slope from the Arctic Ocean to the North
Atlantic, transporting water masses of Arctic origin and sea ice. The West Spitsbergen Current, the northward
extension of the Norwegian Atlantic Current, is flowing to the north along the eastern shelf break and slope,
transporting mainly water of Atlantic origin. In Fram Strait part of the flow continues to the Arctic Ocean, while
another part of the Atlantic Water recirculates and joins the EGC, thereby subducting below the Polar Surface
110   Water (Quadfasel et al., 1987; Hattermann et al., 2016; von Appen et al., 2015).

Sea ice is transported with the EGC from the Arctic Ocean to the Nordic Seas. During winter in the western
Nordic Seas also ice formation takes place. The ice primarily covers the western shelf and only in extreme
winters reaches the deep GS (Comiso et al., 2001; Comiso et al., 2008; Comiso and Hall, 2014).

115

2.2 Seagliders

Seagliders are buoyancy-driven autonomous underwater vehicles that move through the water in a sawtooth
120   pattern between the sea surface and a prescribed dive depth (Davis et al., 2003; Rudnick et al., 2004). Data are
recorded during the dive and climb (down- and upward motion) and transmitted via satellite to the basestation
during every surfacing. At that time the glider can receive commands concerning his flight behavior and
direction and his way of data sampling. Typically, the glider is instructed by a target file, containing waypoints,
about the planned courses of the mission, and by a science-file about the sampling frequencies for the different
125   sensors (see Table 1 and Section 3.1 with Table 2). New command files are sent if tuning of the flight behavior is
needed.

For a given dive depth and dive time the glider's internal flight model calculates the needed buoyancy change
and trim of the instrument for a sawtooth-pattern of down- and upward motion in direction to the next waypoint.
130   The hydrodynamic shape and the small fins of the glider support the realization. The flight model additionally
calculates the vertical velocity of the glider during dive and climb, which is used in the post-processing of the
data. During every surfacing, the flight model compares the calculated position with the real one determined by
GPS. From the discrepancy the depth-averaged current is calculated. If requested these depth averaged current
can be used during the following dives in the flight model for an advanced calculation of the course to the next
135   waypoint. If water depths lesser than the prescribed dive depth are expected information from altimeter bottom
tracking can be used for the ending of the downward motion.

The buoyancy of the glider is changed by changing the volume through inflation/deflation of an oil bladder
(similar to profiling floats). The pitch (downward/upward orientation of the instrument) is changed by
140   repositioning the center of mass by moving the battery pack forward/backward. To control the roll of the

instrument (turn to the left/right) an additional weight is fixed axial asymmetric at the battery pack. By turning the battery to the right or left, in glider is turning accordingly.

Deep and slow dives need less energy and thus allow longer missions than shallow and fast dives; furthermore they allow better steering between waypoints. On the other hand, shallower dives increase the horizontal resolution and faster dives allow capturing sections in shorter time. Seagliders were used in the described missions because high energy supply is characteristic for this type of gliders. The used instruments are restricted to work in ice-free water.

2.3 The missions

During summers 2014 and 2015, Seaglider missions were carried out in the western GS. The measurements started with an east to west section in 2014, but later concentrated on a southeast to northwest section (Fig. 2) perpendicular to the bathymetry (from 75°N/2°W to 76°N/6°W in 2014 and to 76°30'N/7°20'W in 2015). Table 1 summarizes information about both missions.

Table 1: General information on the two glider missions in summer 2014 and summer 2015

year	2014	2014	2015
glider SN	127	558	127
deployment	2014/06/30 75°00'N, 0°00'E/W with RV Polarstern (PS85)	2014/07/01 75°00'N, 0°01'W with RV Polarstern (PS85)	2015/07/14 75°45'N, 3°08'W with RV Polarstern (PS93.1)
recovery	2014/09/13 74°31'N, 1°58'W with MV Plancius *	2014/09/04 73°45'N, 16°16'W with MV Ortelius *	2015/10/05 75°45'N, 3°08'W with RV Polarstern (PS94)
E-W sections	dive 1-101	dive 1-120	
SE-NW sections	dive 101-220	dive 120-358	dive 1-420 northern sect: dive 282-343 shelf-dive 128-151, 257-270, shelf-dive with altimeter bottom tracking: 292-316
		to recovery position (NE to SW) dive 359-484	
	2014/08/21 voltage-cutoff; surface drift until recovery		
total	220 dives 52 days 179 dives to 1000 m 41 dives ≤ 500 m typical distance for 500/1000 m dives: 2.8/3.8 km total mission distance: 910 km	484 dives 65 days 142 dives to 1000 m 342 dives ≤ 500 m typical distance for 500/1000 m dives: 2.1/4.0 km total mission distance: 1266 km	420 dives 84 days 500 m ≤ 329 dives ≤ 1000 m 91 dives ≤ 500 m typical distance for 500/1000 m dives: 1.7/4.8 km total mission distance: 1678 km

* We gratefully acknowledge the support by OCEANWIDE EXPEDITIONS.

The focus of the project is on the near-surface hydrography and thus high horizontal resolution in the upper part of the water column is of foremost interest. Nevertheless, because of its unstable flight behavior during summer 2014 glider 127 was set to dive nearly always to 1000 m depth to achieve good steering. Glider 558, which had a more stable flight, was set for more than 70 % of the dives to 500 m depth. During summer 2015, glider 127 had

a very stable flight. Thus, it was programmed to dive only to 500 m depth or to smaller depths on the shelf. There altimeter bottom tracking kept the glider 50-100 m above the bottom.

170

2.4 The ice situation

Until middle of July, the ice situation in the observation site was quite similar in 2014 and 2015 (Fig 3): the broad shelf east of Greenland was covered with ice and the ice reached at least the position of the 1000 m depth

175 contour. In the months after July, however, the ice coverage evolved differently in the two years.

In 2014, the ice between the perennial fast ice east of Greenland (Schneider and Budéus, 1995) and the central Fram Strait reduced continuously until September. Nevertheless, during the whole summer an ice tongue remained above the shelf break and the upper slope. Thus the ice edge, located above deep waters, was always

180 reached by the gliders at the northeastern-most position of the glider sections. But the ice tongue prevented the glider to be operated across the EGC and to the shelf.

In 2015, a similar gap between the fast ice east of Greenland and the ice coverage in Fram Strait developed. But in that year the shelf break and slope have been completely ice-free from mid-July to mid-September. Large part

185 of the shallow shelf was also ice-free, but was ice-covered again already beginning of September. This situation gave the opportunity to extend the sections to the shelf. With altimeter bottom tracking a number of dives were carried out at around 300 m bottom depth. In August a more northern line across the shelf break to the inlet of the Norske Trough (Arndt et al., 2015) was executed. However, since the navigation of Seagliders in shallow water is problematic, the ice edge was never reached in 2015.

190

Figure 3: The development of the ice cover in the western Greenland Sea from Fram Strait to 72°N; left column for summer 2014, right column for summer 2015; month and day of the ice concentration are given in the upper left corner. The maps base on ice concentration data made available during the missions by DRIFT&NOISE (driftnoise.com). For each year, a sketch of the respective glider sections is added to the map. Black contours give the 3000 m, 1000 m and 300 m depth contour based on RTOPO2 (Schaffer et al., 2016). The location of the map is shown as inlet in Fig. 1 with a blue dashed line.

195
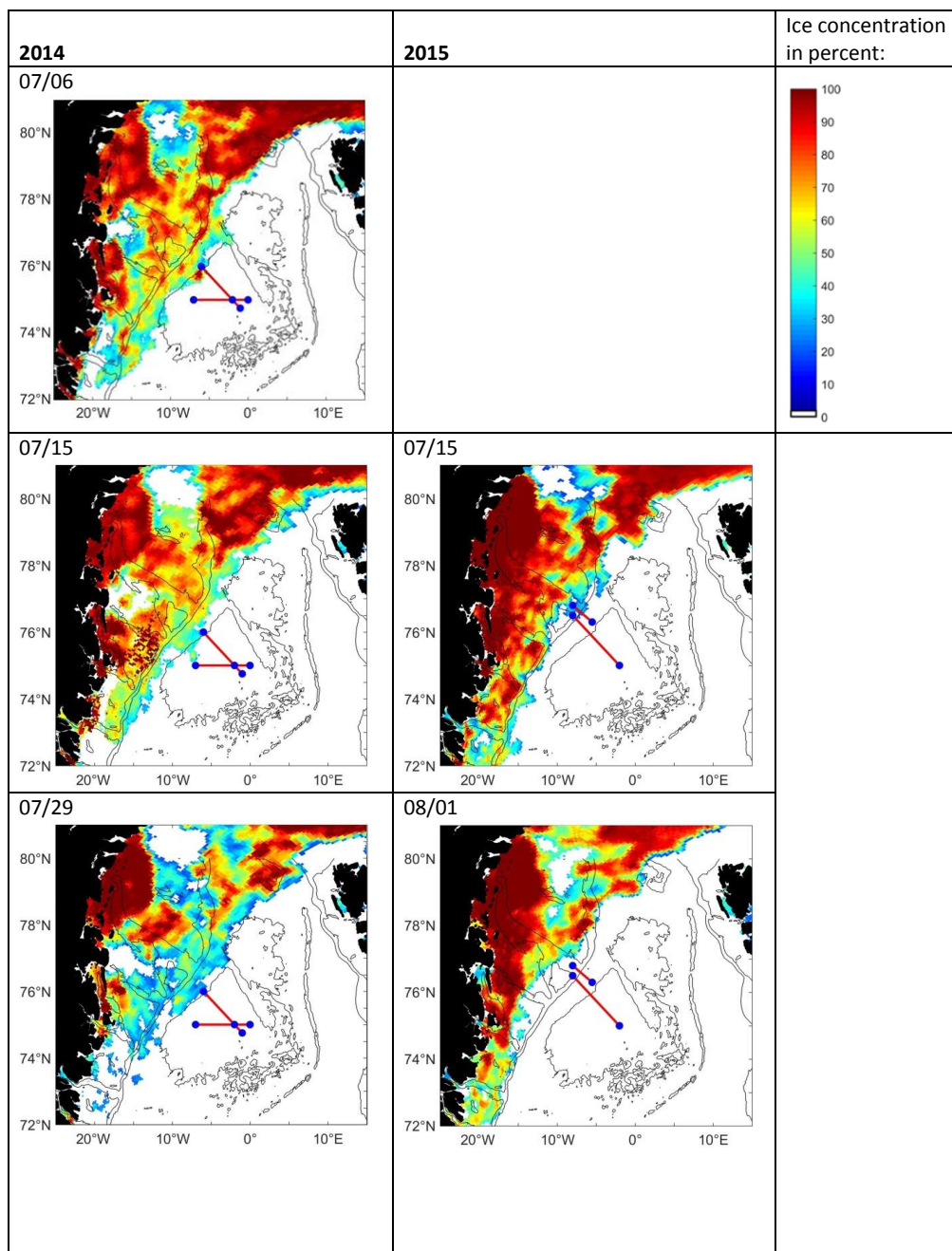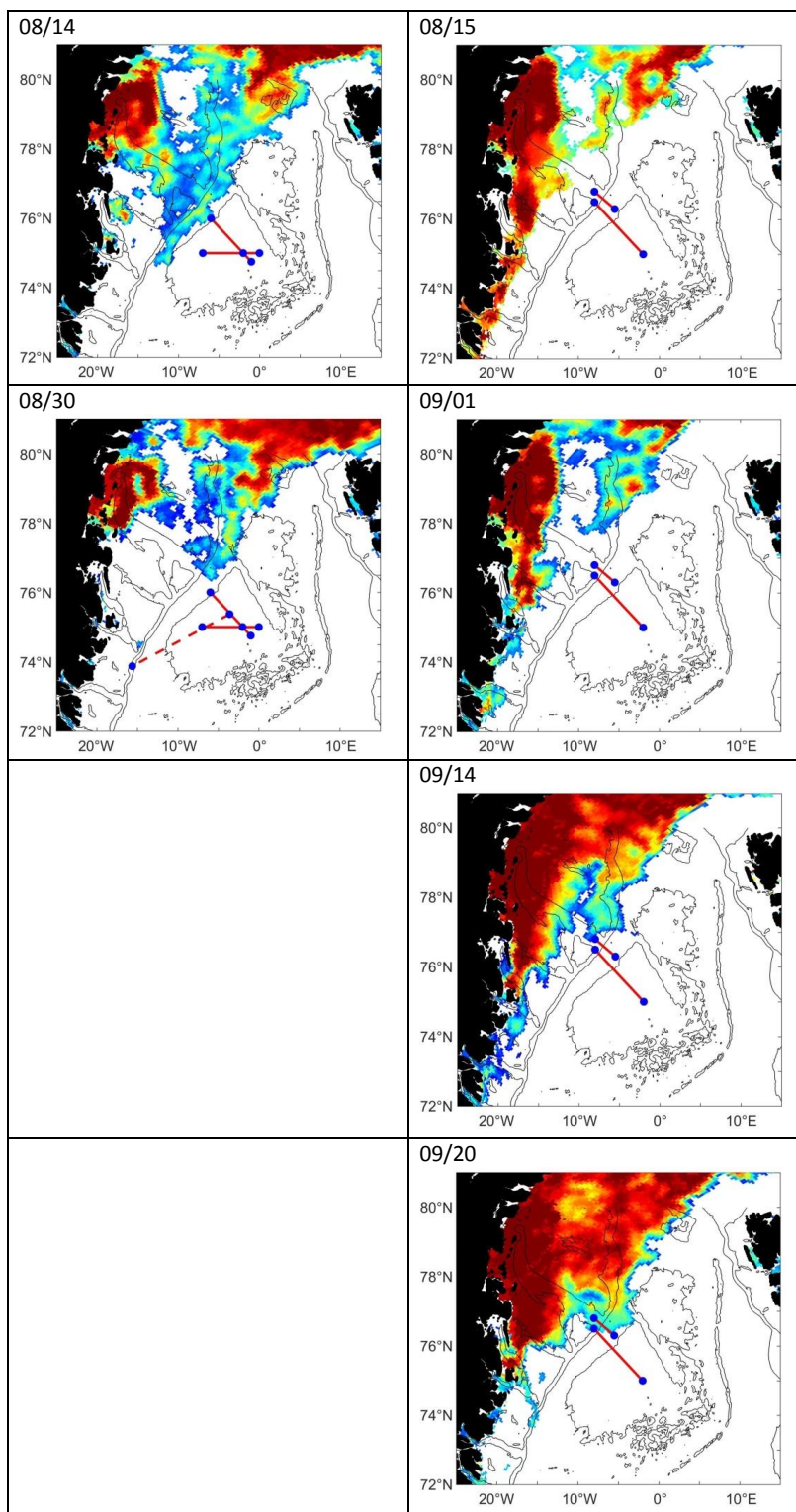
3 Data and processing

3.1 Glider setup, data transfer and raw data

The gliders were equipped with sensors for temperature, conductivity, pressure, oxygen and optical parameters (Table 2). However, during the missions, only temperature, conductivity and pressure data were recorded. Temperature and conductivity sensors have been calibrated by Sea-Bird (www.seabird.com) before the missions. The communication with the gliders was performed via Iridium satellites and a basestation run by the company Kongsberg (www.km.kongsberg.com, https://usermanual.wiki/Document/4900039BasestationUserGuide.3614056780.pdf). The piloting was carried out by a team in the section Polar Oceanography at the Alfred Wegener Institute, Helmholtz Centre for Polar and Marine Research (AWI) with support from Optimare, Harald Rohr.

During every surfacing, the data of the gliders were sent ashore. On the basestation, the data of each dive were decoded and transformed into two files containing the scientific data (eng file) and the technical data as well as information about the setting of the piloting parameters (log file), respectively. These files were the basis for the real-time analysis of the glider performance. If changes of the flight behavior were necessary the pilots submitted new command files to the basestation, which were transferred to the glider during the next surfacing. Sometimes also new target files were sent for changes in the planned track or new science-files for changes in the sampling of the sensors. Also the data processing is based on the eng and log files.

Table 2: Origin of the gliders 127 ad 558 and their setup during the two missions in the Greenland Sea in summer 2014 and summer 2015.

glider sn	127	558
manufacturer	University of Washington	iROBOT
year of delivery	2006	2012
missions presented here	2014, 2015	2014
sensors	conductivity, temperature: SBE CT sail, SN 0050, unpumped pressure: Druck PCDR 4020, SN 2438976 chlorophyll, CDOM, scattering: Wet Labs Optics, SN BB2fVMG-163 oxygen: Aanderaa Optode AA 3830, SN: 11 altimetry: Applied Acoustic Engineering Seabed Transponder 955, SN 021/761	conductivity, temperature: SBE CT sail, SN 0190, unpumped pressure: Paine 211-75-710-05, SN 269511 chlorophyll, CDOM, scattering: Wet Labs Optics, SN BB2FLVMT-87 altimetry: Applied Acoustic Engineering Seabed Transponder 955, SN 283/2444
sampling	0 – 1000 m: conductivity, temperature and pressure every 5 sec (Wet Labs Optic data and oxygen data were not sampled)	0-1000 m: conductivity, temperature and pressure every 5 sec (Wet Labs Optic data were not sampled)

3.2 Development of an own data processing

The glider data are comparable to data from ship-based CTD measurements. Thus the processing for these data follows basically the processing for ship-based CTD data. The aim of the processing is to eliminate random erroneous data, to correct systematic erroneous data and finally deliver profiles of temperature, conductivity,

salinity and density on regular pressure steps. Expected systematic errors are a miss-alignment between temperature and conductivity measurements (time lag) (see for example Morison et al., 1994), a long-term distortion of the conductivity measurements (thermal lag) (Garau et al., 2011) and problems with the applicability of the sensor calibration as the latter was conducted before the sensors were mounted on the

235   instrument.

For a proper calculation of salinity and density, temperature and conductivity measurements from the same water body are needed. Otherwise spikes occur, especially if the glider was diving trough strong gradients. Due to different response times and different placement of the sensors on the instrument, different water bodies were measured byt the temperature and conductivity sensors at the same time. This time lag was corrected by an

240   alignment of temperature and conductivity data, which involves a vertical interpolation of the measured conductivity values.

The thermal lag, induced by the different geometry and heat capacity of the cells, was corrected in a second step. This error lasts over several consecutive measurements. The correction was derived from the original data but it

245   failed if extreme outliers were still present in the data.

Glider CTD data are more distorted than ship-based CTD data because

1. The vertical resolution of the glider measurements is low compared to that of a ship-based CTD.

250   The gliders sample with 0.2 Hz (every 5 sec). With a typical vertical velocity of 0.1 to 0.12 m/s this results in a vertical resolution of approximately 0.6 dbar (3-4 values in a layer of 2 dbar).

A ship-based CTD samples with 24 Hz (every 0.04 sec) and is typically lowered at 0.5 to 1 m/s, resulting in a typical resolution of 0.02 dbar (48-96 values in a layer of 2 dbar).

2. The vertical velocity of a glider is much more variable than that of a lowered CTD, because the change

255   in buoyancy (which accelerates the glider) is calculated with the flight model using a prescribed vertical density structure. The latter might deviate from the real local density structure. Due to the lower sampling rate information about the vertical velocity of the instrument is also much coarser for gliders than for ship CTDs. .

3. The water is not pumped through the glider's conductivity cell but the cell is free-flushed, because of

260   limited energy resources. Thus the calculation of the flushing time depends on the uncertain vertical velocity (see 2.).

4. The quality of the interpolation for the time-lag correction depends on the vertical resolution, the information about the vertical velocity and the flushing time of the cell (see 1., 2. and 3., and Alvarez (2018) for numerical analysis of the performance of unpumped SBE sensors at low flushing rates).

265 5. The thermal-lag correction depends on the geometry and flushing time of the conductivity cell (see 2. and 3.).

6. The sensors are calibrated before mounting them on the glider, which limits the applicability of the calibration.

270   For these reasons glider data are much noisier and the time-lag- and thermal-lag-correction are of lower quality for glider CTD data than for ship-based CTD data. With respect to these problems, a data processing was set up at AWI, which consists of two parts (Table 3).

First, the raw data, as provided by the KONGSBERG basestation, were transformed to physical units and
275   merged with the pre-mission calibration information. Corrections were applied to the data according to information from the gliders flight model and for the time lag and thermal lag of the sensors. This part was done by means of the UEA Seaglider Toolbox (UEA: University of East Anglia, Norwich, http://www.byqueste.com/toolbox.html). In addition to that, an extended processing was developed and applied to the glider data to exclude erroneous data, interpolate the data to discrete pressure levels, smooth the derived
280   quantities and adjust absolute temperature and salinity to data from high-precision ship-based CTD casts close to the glider mission in space and time. It was also analyzed if down- and upcast data show systematic discrepancies and thereupon it was decided if they can be used both or not. This second part of the processing involved knowledge of the regional hydrographic conditions. A prerequisite for a proper functioning of the thermal lag correction is the exclusion of erroneous data/spikes. Thus, the first and second part of the processing
285   are entangled.
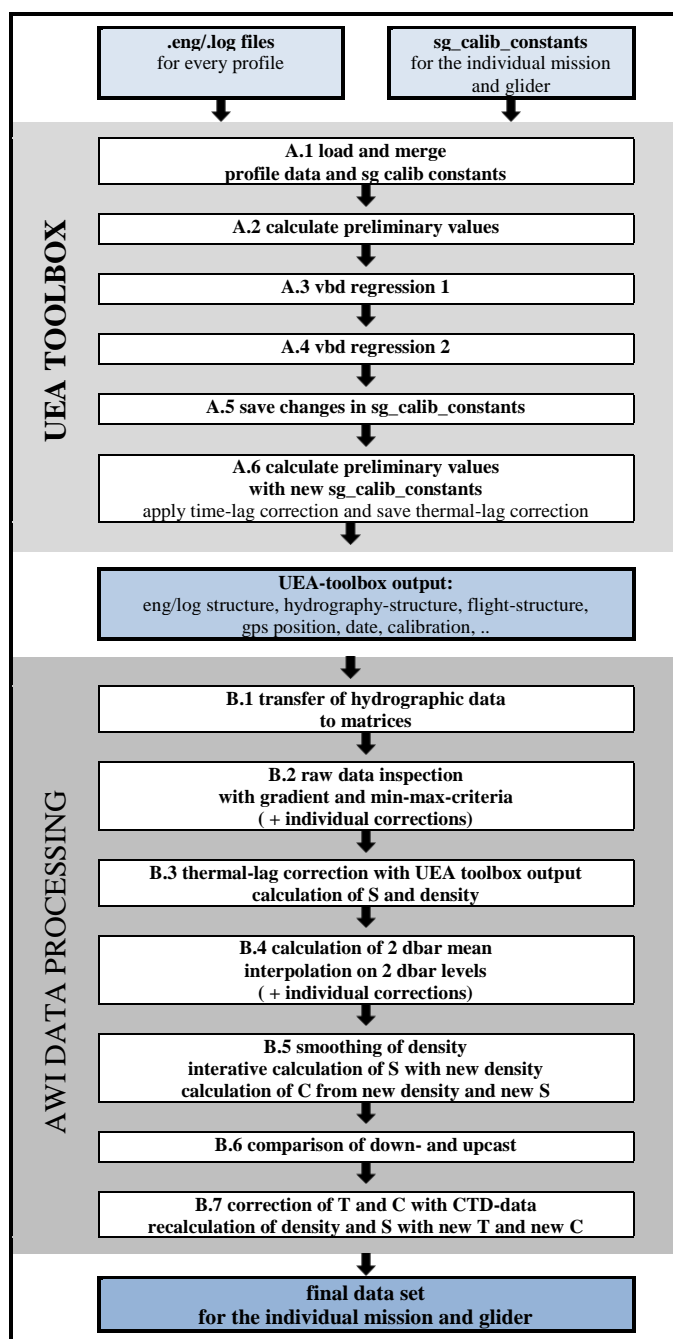
Table 3: Flow chart of glider data processing with UEA toolbox and AWI additions. For each individual profile the eng and log files contain the scientific and technical data. The sg_calib_constants-file contains the information about the pre-deployment calibration of the individual gliders.

sg_calib_constants – file containing calibration information, vbd – vertical buoyancy divice, UEA – university of East Anglia, T- temperature, S – salinity, C – conductivity.

290

3.3 Description of the data processing

The individual steps of Table 2 are described in the following.

A   UEA toolbox

A.1   load and merge profile data and sg calib constants

The information from eng and log files (see Section 3.1) as well as from the sg_calib_constants-file
was merged in a matlab-file. The sg_calib_constants-file contains the information about the calibration
constants of the individual glider; sg – Seaglider.

A.2   calculate preliminary values

Preliminary values of the flight characteristics as well as temperature, conductivity and derived
variables such as salinity and density and corrected pressure for each sensor were calculated. Based on
the information about the calibration constants from the sg_calib_constants-file the frequency
measurements for temperature and conductivity were transformed into physical units.

The movement, and thus the exact position, of the glider under water was derived from a flight model.
These data were corrected by comparing the vertical velocity of the glider, calculated as change of
pressure with time, with the flight model vertical velocity. The correction of the flight model has
influence on derived variables such as dive-averaged currents, but also on the calculation of
conductivity. In two steps various parameters were fitted so as to minimize the difference between the
vertical velocities (Frajka-Williams et al., 2011).

A.3   vbd regression 1

(vbd: variable buoyancy device)

The maximum volume of the instrument was determined during pre-deployment tank tests and the
reference environmental density was calculated from expected temperature and conductivity values for
the mission region. Both values were adjusted to minimize differences between the flight-model
vertical velocity and the observed vertical velocity.

A.4   vbd regression 2

The parameters of the hydrodynamic model were adjusted to minimize differences between the
observed upward and downward velocities.

A.5   save changes in sg_calib_constants

During the vbd regression 1 and 2 (A.3 and A.4) some glider-specific parameters were changed. The
changes were saved in the sg_calib_constants-file.

A.6   calculate preliminary values with new sg_calib_constants

See A.2; values of the flight characteristics as well as temperature, conductivity and derived variables
such as salinity and density and corrected pressure for each sensor were recalculated after changes in
the sg_calib_constants-file have been made.

Apply time-lag-correction and save thermal-lag correction

The time-lag-correction calculated from the UEA-toolbox was applied to the data. The thermal-lag
correction was calculated from the UEA-toolbox but not applied to the data set at this step. Before a

thermal lag correction erroneous data/spikes must be removed. The thermal-lag-correction was saved and applied at step B.3.

For details of the UEA toolbox see:

http://www.byqueste.com/toolbox.html

295

B   AWI data processing

B.1   transfer of the hydrographic data from the UEA-toolbox output from matlab-structures to matrices

B.2   raw data inspection with gradient and min-max-criteria
(+ individual corrections)

To eliminate spikes, data were deleted, when the difference between temperatures or conductivities of consecutive levels was larger than 0.25 °C or mS/cm, respectively. This gradient criterion was only applied below the thermo- or halocline.

Also all unrealistic data were deleted. The limits were temperatures lower than -2°C and higher than 15°C, conductivities lower than 23 mS/cm and higher than 38 mS/cm. These limits were chosen on the background of local hydrography.

The mean vertical velocity (w) during the dives was between 10 and 12 cm/s. Lower velocities occurred at the start of the dive, in the apogee between down- and upward motion and at the end of the dive, but could have also occured if the trim of the glider was wrong resulting in a slower vertical movement than normal. During these phases of low speed, the conductivity measurements can be wrong because of air bubbles in the water and insufficient flushing of the cell. Thus, data lines with vertical velocity smaller than 5 cm/s were deleted.

B.3   thermal-lag correction with UEA toolbox output
Calculation of salinity and density

The conductivity was corrected for thermal-lag according to the UEA toolbox output from A.6. Salinity and density were recalculated with the corrected conductivity.

Finally pressure, temperature with time-lag correction, conductivity with thermal-lag correction and the derived quantities salinity and density were saved.

B.4   calculation of 2 dbar mean
interpolation on 2 dbar levels
(+ individual corrections)

To reduce the noise, the data were averaged within depth levels. Since we are interested to analyze the distribution of freshwater in the near-surface layer with a typical thickness of 5 to 25 dbar, we chose 2 dbar as the interval for calculation of mean values, which were then interpolated to discrete depth levels every 2 dbar from the surface to the dive depth. This vertical resolution was a compromise between a sufficient vertical resolution and the reliability of the mean values (see Section 3.2, 1. for details)

In the final data set the variable numrec gives the number of records from which 2 dbar-means were

calculated.

B.5   smoothing of density

iterative calculation of salinity with new density

calculation of conductivity with the new density and the new salinity

Salinity and density, calculated from the interpolated temperature, conductivity and pressure (B.4) were still very noisy. This was due to the lesser measurement accuracy of conductivity in relation to temperature, caused by the size of the conductivity cell. Particularly there were small instabilities in the density stratification. Thus, density was filtered by a running mean over 11 layers (22 dbar). Afterwards salinity was iterative changed in steps of 0.000065 until the respective calculated density reached the density from running mean within $\pm$ 0.000125 kg/m³. Finally, for data consistencies conductivity was recalculated from temperature, pressure and new salinity.

B.6   comparison of down and up casts

Since the CTD sensors are mounted on the top of the main body of the glider they are equally flushed during the down- and upward motion. Consequently, profiles from both directions can be used. This is other than for ship-based CTD data, where only down-casts are used. Nevertheless, sometimes systematic discrepancies between down and up profiles have been reported (Garau et al., 2011). Fortunately for none of the missions reported here, systematic differences between down and up-casts were visible. Thus, data from both casts were stored in the final data set. The direction of the cast is archived as the parameter direction: D: down, U: up.

B.7   adjustment of temperature and conductivity with ship-based CTD-data;

recalculation of salinity and density with new temperature and new conductivity

During the deployment of each glider, a ship-based CTD cast was carried out. The ship-based CTD temperature and conductivity data between 500 and 1000 dbar were compared with the mean temperature and conductivity profiles of all glider data in the same depth range within a spatial distance of $\pm$ 0.5 ° in longitude and $\pm$ 0.25 ° in latitude (i.e. approx. 30 km). Average differences in temperature and conductivity were calculated and all glider profiles were corrected by these offsets.

* individual corrections

The data processing steps listed above were not able to remove a number of individual errors:

- spikes, especially in the depth range of the thermo/halocline
- wrong values during the apogee, which were not removed by the criterion w < 5 cm/s
- outlier profiles of conductivity
- profiles with large gaps in the depth of the largest gradient
- incomplete profiles, because the dive was aborted by the glider-intrinsic software after an

uncommanded change in the bleed counts of the vertical buoyancy device

The wrong data lines or even the whole profiles were removed before the interpolation to 2 dbar levels took place.

3.4 Quality of the data set – reasons for and effects of the different steps of the data processing

3.4.1 CT sail specification:

Sea-Bird temperature sensor and free-flushed conductivity sensors, referred to as the CT sail, were installed on Seagliders 127 and 558. The CT Sail consists of three parts, the "CT" temperature sensor and conductivity cell, the temperature circuit board and the conductivity circuit board. These parts were disassembled and reassembled each time the CT Sail was calibrated and afterwards installed into the glider again. The calibration was conducted in advance to both missions. As the process of disassembly and assembly was not within the control of Sea-Bird, the applicability of the calibration is limited.

The specification of the CT sail:

 initial accuracy: conductivity $\pm$ 0.003 mS cm^{-1}, temperature $\pm$ 0.002°C

typical stability: conductivity $\pm$ 0.003 mS cm^{-1} per month, temperature $\pm$ 0.0002°C per month

(comparable to SBE 37, Sea-Bird Electronics: www.seabird.com)

3.4.2 Errors introduced by an insufficient time-lag correction:

(data processing step A.6)

Errors in the form of spikes in salinity occurred when the gliders moved through sharp gradients. The spikes were produced by insufficient alignment between temperature and conductivity in relation to pressure. Negative spikes were expected if the conductivity measurement was before the temperature measurements and positive spikes if conductivity laged temperature (seabird software documentation: https://www.seabird.com/cms-portals/seabird_com/cms/documents/training/ Module12_AdvancedDataProcessing.pdf). In our glider profiles both kind of spikes were visible within one profile, reflecting variations in the vertical velocity of the glider. Thus, the systematic alignment of temperature and conductivity was not successful at whole. Additionally the vertical resolution of the measurements did not enable an adjustment of the time lag correction. For ship-based CTD measurements typical adjustment is of approximately 20-30 msec for 50 cm/s vertical velocity and 24 Hz sampling. This is equivalent to an alignment correction of 1 cm equivalent to 0.01 dbar for conductivity. To apply such a correction, the resolution of the original ship-based conductivity measurements has to be doubled by interpolation. If similar adjustment should be applied to the glider data, the vertical resolution would have to be refined with interpolation between measured values by a factor of 60 as on average the glider samples every 0.6 dbar. Especially in the region of sharp gradients we did not expect a good approach of the gradient by this refinement and hereupon no improvement of the time-lag correction. Thus, we decided to leave these spikes uncorrected. Example spikes are shown for the glider 127 during the mission in 2015 in Fig. 4. They are of order $\pm$ 0.05 to 0.1 in salinity.

Queste et al. (2016) developed a method to deal with glider measurements across sharp gradients. They built composite profiles from the downcasts between the surface and the thermo-/halocline and from the upcasts between maximum depth and thermo-/halocline and combined these in a gridded data set.
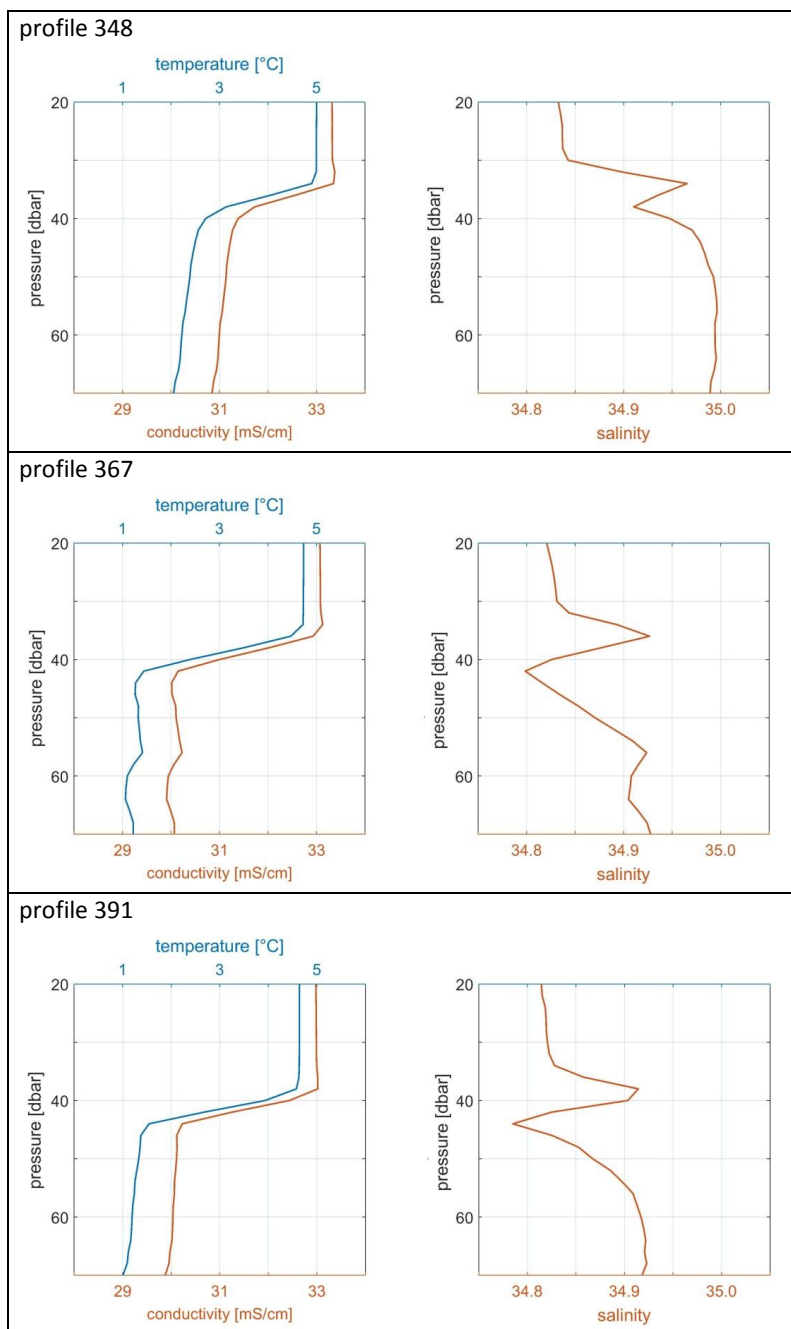
Figure 4: Exemplarily, three temperature, conductivity and salinity profiles from glider 127 during summer 2015 demonstrate how spikes in salinity show up in the depth of highest vertical gradient between the surface layer and the water masses below. These spikes are generated by an insufficient time lag correction (see Section 3.4.2 for details).

345

3.4.3 Visual inspection of the temperature, conductivity, salinity, density and vertical velocity profiles

350   (data processing step *individual corrections*)

By visual inspection of all individual profiles at different steps of the processing, several individual faulty values or profiles are detected. These are removed from the data set. It effects a reduction of the original data sets between 2 % and 5% (see Table 4).

355   **3.4.4 Smoothing of the profiles**

3.4.4.1 Averaging the original measurements over 2 dbar intervals

(data processing step B.4)

360   As described above (Section 3.4) the original measurements were averaged over 2dbar to reduce the noise of temperature and conductivity. The 2dbar mean values were on average based on 3 or 4 original data. Figure 5 shows the number of values for the averages and the standard deviations, exemplarily for glider 127 during the mission 2015 (for glider 127 and 558, mission 2014, the figures look similar).

365   There was a small difference in the number of records between the down- and upcast due to slightly different velocities. The reduced numbers at the maximum depth of the profiles and at the beginning of the downcast reflect the rejection of data during the start of the dive and during the apogee/bottom dead point, where the vertical velocity was below 5 cm/s. Larger numbers at the surface reflect measurements before the profile was started.

370

The standard deviations are below 0.01 °C for temperature respectively 0.01 mS/cm for conductivity below 200 dbar depth, but up to 0.12 °C respectively mS/cm between 30 and 40 dbar, reflecting the strong temperature and salinity gradients belonging to the thermo-/halocline. For conductivity we additionally have an outstanding high standard deviation near the surface of up to 0.38 mS/cm. Near the surface there is a high risk that measurements

375   of the conductivity are falsified by air bubbles (see Section 3.2, 3.). Unrealistic values have been excluded *(*Section 3.4.3).
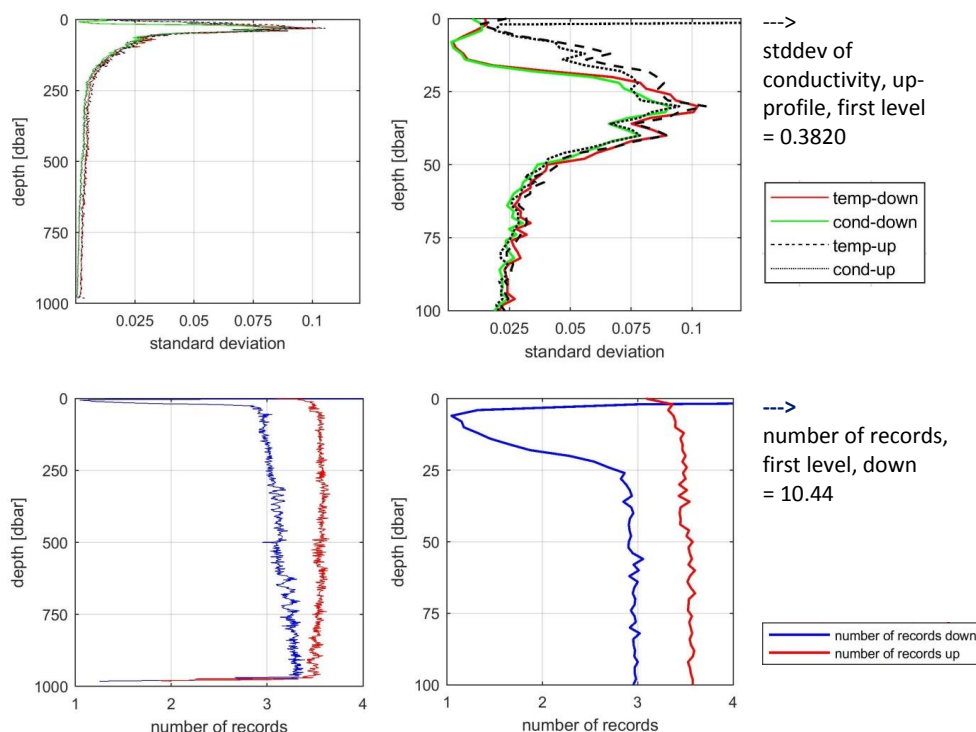
380

Figure 5: Standard deviation (top) and number of original data (bottom) for 2 dbar averages of temperature and conductivity are examplarily shown for the down- (red) and upcasts (green) of glider 127 during the mission 2015. On the left the total profile is shown, in the middle only the upper 100 dbar of the profiles. Extreme values at the surface and the legend for the figures to the left are given in the right
385 **column.**

3.4.4.2 Smoothing of density and salinity

390   (data processing step B.5)

To quantify the noise reduction of step B.5 where the criteria of stable density was applied we calculated the variability of a profile before and after the step. The variability is here defined as the difference between consecutive values of salinity in a profile. Figure 6 shows the variability for all individual salinity profiles, again exemplarily for glider 127 during the mission 2015. Apart from the upper layers the variability was reduced by
395   50 % with step B.5.
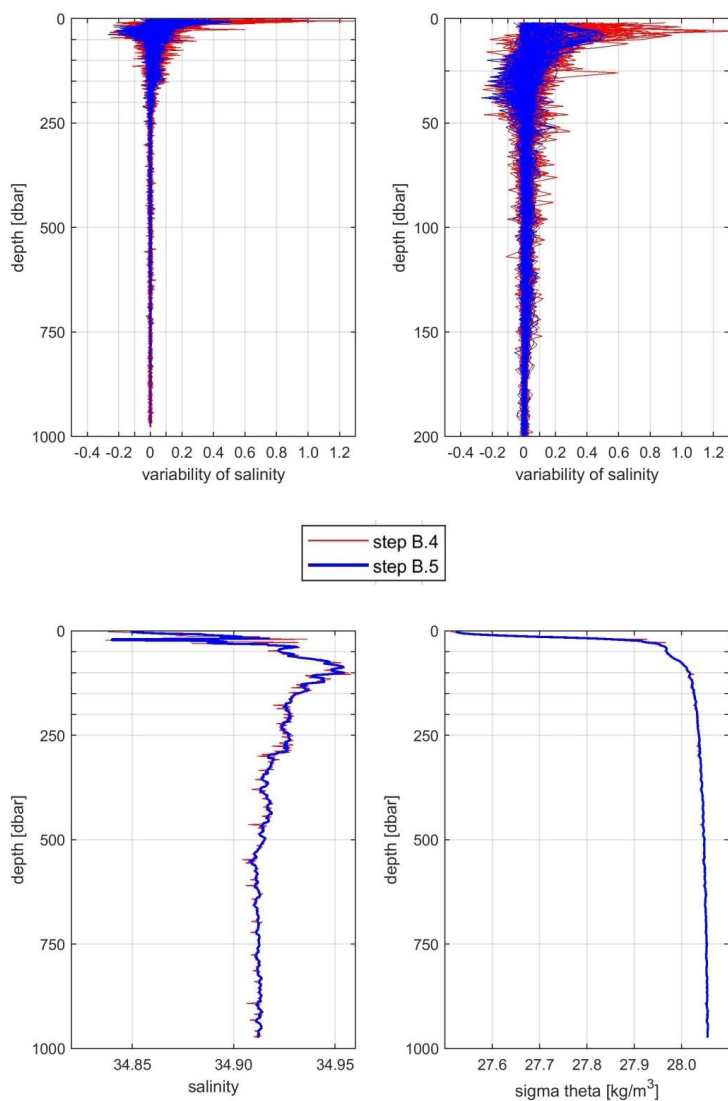
Figure 6: (Top) Variability for all individual salinity profiles before (red) and after (blue) smoothing of density, (left) for the total profile depth, (right) for the upper 200 dbar; again exemplarily for glider 127, mission 2015.(Bottom) an individual salinity (left) and density (right) profile before (red) and after (blue) smoothing of density.

3.4.5 Adjustment of absolute values to ship-based CTD data

(data processing step B.7)

The adjustment of absolute values to ship-based CTD data was at least an order of magnitude larger than the accuracy of an SBE 37 and thus demonstrate the urgent need of high-quality ship-based CTD data in the vicinity of a glider mission.

Values for the different inaccuracies are summarized in Table 4.

Table 4: Summary of the data quality and effects of the different steps of the data processing for the three individual data sets (glider 127 mission 2014, glider 558 mission 2014 and glider 127 mission 2015). References to the specific steps of the data processing are given in the left column.

415

	glider 127 mission 2014	glider 558 mission 2014	glider 127 mission 2015
specification of CT sail (see Section 3.4.1)	initial accuracy: conductivity ± 0.003 mS/cm temperature ± 0.002 °C typical drift: conductivity ± 0.003 mS/cm per month temperature ± 0.0002 °C per month		
spikes not eliminated by time-lag-correction (see Section 3.4.2)	± 0.05 to 0.1 in salinity		
data reduction with gradient/min-max criterion and individual corrections (step B.2 and B.3, see Section 3.4.3)	5 %	2.2 %	4 %
standard deviation of 2 dbar averages (step B.3, see Section 3.4.4.1)	temperature 0-80 dbar 0.06 °C 80-1000 dbar 0.004 °C 0-1000 dbar 0.009 °C conductivity 0-80 dbar 0.05 mS/cm 80-1000 dbar 0.002 mS/cm 0-1000 dbar 0.007 mS/cm	temperature 0-80 dbar 0.06 °C 80-1000 dbar 0.003 °C 0-1000 dbar 0.007 °C conductivity 0-80 dbar 0.05 mS/cm 80-1000 dbar 0.003 mS/cm 0-1000 dbar 0.007 mS/cm	temperature 0-80 dbar 0.05 °C 80-1000 dbar 0.006 °C 0-1000 dbar 0.009 °C conductivity 0-80 dbar 0.06 mS/cm 80-1000 dbar 0.004 mS/cm 0-1000 dbar 0.008 mS/cm
number of records for 2 dbar averages:	3.5	3.2	3.3
variability reduction of salinity (step B.4, see Section 3.4.4.2)	0-80 dbar 0.051 → 0.046 80-1000 dbar 0.0019 → 0.0007 0-1000 dbar 0.0058 → 0.0045	0-80 bar 0.073 → 0.067 80-1000 dbar 0.0011 → 0.0006 0-1000 dbar 0.0069 → 0.0060	0-80 dbar 0.028 → 0.025 80-1000 dbar 0.0046 → 0.0031 0-1000 dbar 0.0025 → 0.0013
comparison with ship-based CTD (step B.5, see Section 3.4.5) diff_T/C/S= temperature/conductivity/salinity difference between glider and ship-based CTD	diff_T=-0.0266 °C diff_C= -0.0104 mS/cm (diff_S=0.0163, not used)	diff_T=-0.0095 °C diff_C= -0.0063 mS/cm (diff_S=0.0024, not used)	diff_T=-0.0389 °C diff_C= -0.0316 mS/cm (diff_S=0.0025, not used)

4 Distribution of temperature and salinity from glider missions

420

This section provides a brief description of the observed temperature and salinity distributions measured during
the two summer glider missions.

Typical hydrographic conditions in the GS reflect the major circulation features in the Nordic Seas. The deep

425   Greenland Basin is bounded by the EGC on the western side. Cold and fresh Polar Surface Waters are
transported with the current from the Arctic Ocean into the subpolar North Atlantic. On the eastern side the
Greenland Basin is bounded by the West Spitsbergen Current. Waters of Atlantic characteristic – warm and salty
– flow along the Norwegian Coast and shelf break to the North and undergo cooling on the way. In Fram Strait
part of the West Spitsbergen Current continues into the Arctic and part recirculates (Rudels et al., 2005;

430   Hattermann et al., 2016). The Recirculated Atlantic Water joins the EGC and partwise subducts below the Polar
Surface Water (see Fig. 1) (Rudels et al., 2002). The central GS is dominated by Arctic Intermediate Waters,
which are relatively cold and salty (Blindheim and Rey, 2004; Rudels et al., 2005; Rudels et al., 2012). The deep
basin of the GS is filled with this water mass, formed by local convection during winter. A very weak
stratification is characteristic for the inner GS, reflecting the winter convection. Strong seasonal variations are

435   only observed on top of the Arctic Intermediate Water. The near-surface layer is dominated by summer
heating/winter cooling. Additionally during late spring and summer occasional freshening is observed (de Steur
et al., 2015; Latarius and Quadfasel, 2016).

Our observations with the gliders captured the Arctic Intermediate Water in the central GS and the Polar Surface

440   Water as well as the Recirculating Atlantic Water near the ice edge in the west, thus confirming the typical
hydrographic conditions. However, only in 2015 the core of the EGC with cold (below -1°C) and fresh (salinity
between 34 and 32) waters down to approximately 100 m was reached (Fig. 7). In 2014 the ice conditions did
not allow to extend the sections that far to the west (see Section 2.4). The West Spitsbergen Current in the east
was never reached.

445

The glider observations give insight into the interannual variability close to the surface. The warm near-surface
layer is around 20 m thick in 2014 but up to twice that thick in 2015 (see Fig. 7). We expect that due to a much
more extended ice coverage the summer heating started later in 2014 (see Section 2.4). But the most obvious
difference between the summers 2014 and 2015 is the near-surface salinity distribution. In summer 2014 waters

450   with very low salinities (31-33) reach up to 3°W, hence occupy two thirds of the section. These waters were
restricted to the upper 10-15 m (see also Fig. 8-10) and only in the north-west, close to the ice edge low salinities
were accompanied by low temperatures. This kind of water most likely was the remnant of locally melted ice (de
Steur et al., 2015).

455   Also in 2015 the lowest salinities in the near-surface layer are at the north-western end of the section. But the
signature is different. The water is restricted to the western end of the section and is not as fresh as in 2014 and
the freshwater is not that concentrated near the surface. As described above it reflects the Polar Surface Water
flowing with the EGC from the Arctic Ocean through Fram Strait to the south and continuing its way along the
shelf break to the subpolar North Atlantic (Rudels et al., 2005). Also the development of the ice coverage during

460   summer 2015 (Fig. 3), suggests that this water mass is not a signature of recent ice melt. Since beginning of
August, the shelf break was not covered with ice. The ice retreated to the shallow shelf close to the coast until
mid-September.

465   All profile data of the final data set along a specific section were gridded in the horizontal at 0.05° longitudinal
resolution (approximately 1.3 km). In the vertical, the profiles were already interpolated to 2 dbar levels during
the data processing.
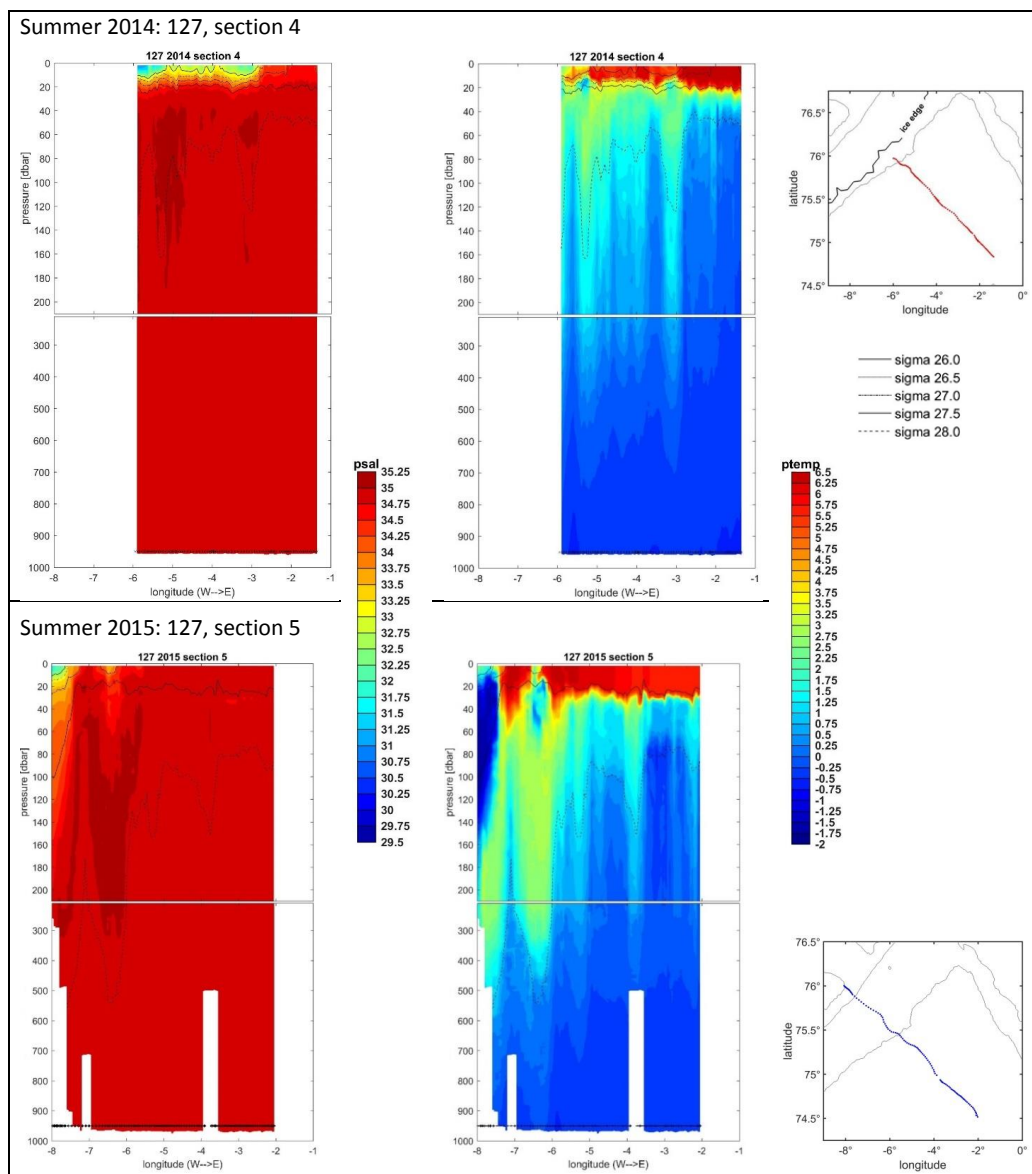
Figure 7: Deep sections (0 to 1000 dbar), exemplarily one for each summer. Left column: salinity, middle column: potential temperature, top: 2014, bottom: 2015. In the right column map extracts show the position of the sections. For 2014 also the ice edge at the arrival time of the glider at the edge is included in the map. During 2015 no ice was observed within the map extract.
Sigma-contours for 26.0/26.5/27.0 and 27.5 kg/m³ are superimposed.
The stars at the bottom of each section mark the position of the profiles before the gridding of the data in the horizontal took place.
Section 4 from glider 127, 2014, from Northwest (left) to Southeast (right); original dives: 168 to 280, profiles 260 to 353 of the final data set, time span August 2 to 8, ice edge information from August 5.
Section 5 from glider 127, 2015, from Northwest (left) to Southeast (right); original dives: 144 to 197, profiles 231 to 336 of the final data set, time span August 11 to 22.

480

Section info	psal	ptemp
Section 1 Dives 1-55 Profiles 1-84 07/01-07/11 <---- Ice edge from 07/11	127 2014 section 1	127 2014 section 1
Section 2 * Dives 60-101 Profiles 93-147 07/11-07/18 ----> Ice edge from 07/11	127 2014 section 2	127 2014 section 2
Section 3 Dives 101-168 Profiles 148-259 07/18-08/02 <---- Ice edge from 08/05	127 2014 section 3	127 2014 section 3
Section 4 Dives 168-220 Profiles 260-353 08/02-08/14 ----> Ice edge from 08/05	127 2014 section 4	127 2014 section 4
Section 5 Dives 221-258 Profiles 359-418 08/14-08/21 <---- Ice edge from 08/19	127 2014 section 5	127 2014 section 5

* section 2, dives 89-104: problems with conductivity sensor		— sigma 26.0 ...... sigma 26.5 -·-·- sigma 27.0 — sigma 27.5 ----- sigma 28.0

Figure 8: Sections: 2014, glider 127, sections 1-5. Shown are the upper 55 m of the water column.
485 **Left column: information and map extract with location of the profiles and ice edge for the time span of the section (see Section 2.4 for details); numbers of original dives on the section, numbers of profiles from the final dataset on the section, time span, and direction of the section: <--- east to west, ---> west to east. Middle/right column: salinity/ potential temperature. Both plots are overlaid with the sigma-contours 26.0, 26.5, 27.0, 27.5 and 28.0 (see legend for line style in Fig. 7). Stars at 50 m depth mark the position of**
490 **the profiles on the section before the gridding of the data in the horizontal toke place. For section 2 many profiles are missing because of problems with the conductivity sensor.**

495

500
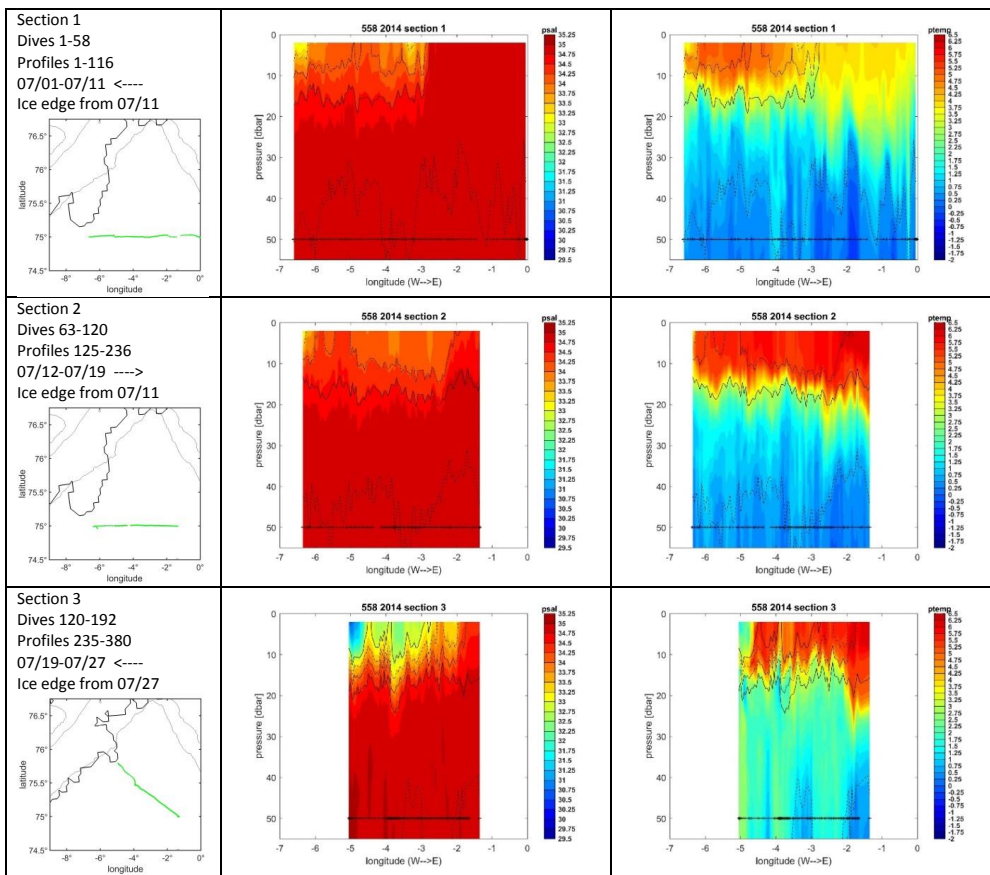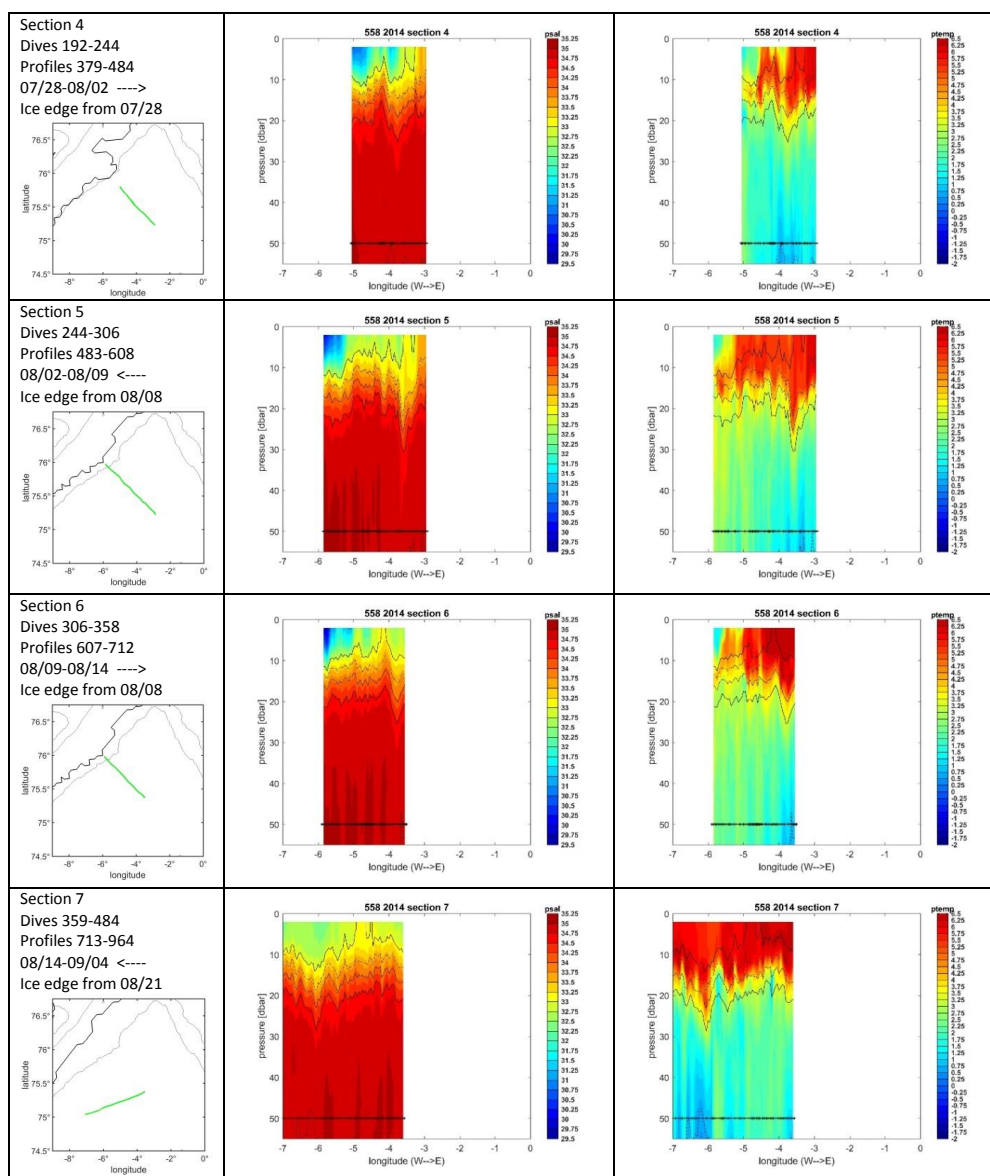
Figure 9: Sections: 2014, glider 558, sections 1-7. Shown are the upper 55m of the water column.
Left column: information and map extract with location of the profiles and ice edge for the time span of
the section (see Section 2.4 for details); number of original dives on the section, number of profiles from
the final dataset on the section, time span, and direction of the section: <--- east to west, ---> west to east.
Middle/right column: salinity/ potential temperature. Both plots are overlaid with the sigma-contours
26.0, 26.5, 27.0, 27.5 and 28.0 (see legend for line style in Fig. 7). Stars at 50 m depth mark the position of
the profiles on the section before the gridding of the data in the horizontal toke place.

Section 2
Dives 22-82
Profiles 42-143
07/18-07/30 <----

Section 3
Dives 82-110
Profiles 142-164
07/30-08/06 ---->

Section 4
Dives 110-144
Profiles 165-230
08/06-08/11 <----

Section 5
Dives 144-197
Profiles 231-336
08/11-08/22 ---->

Section 6
Dives 197-259
Profiles 337-458
08/22-09/03 <----
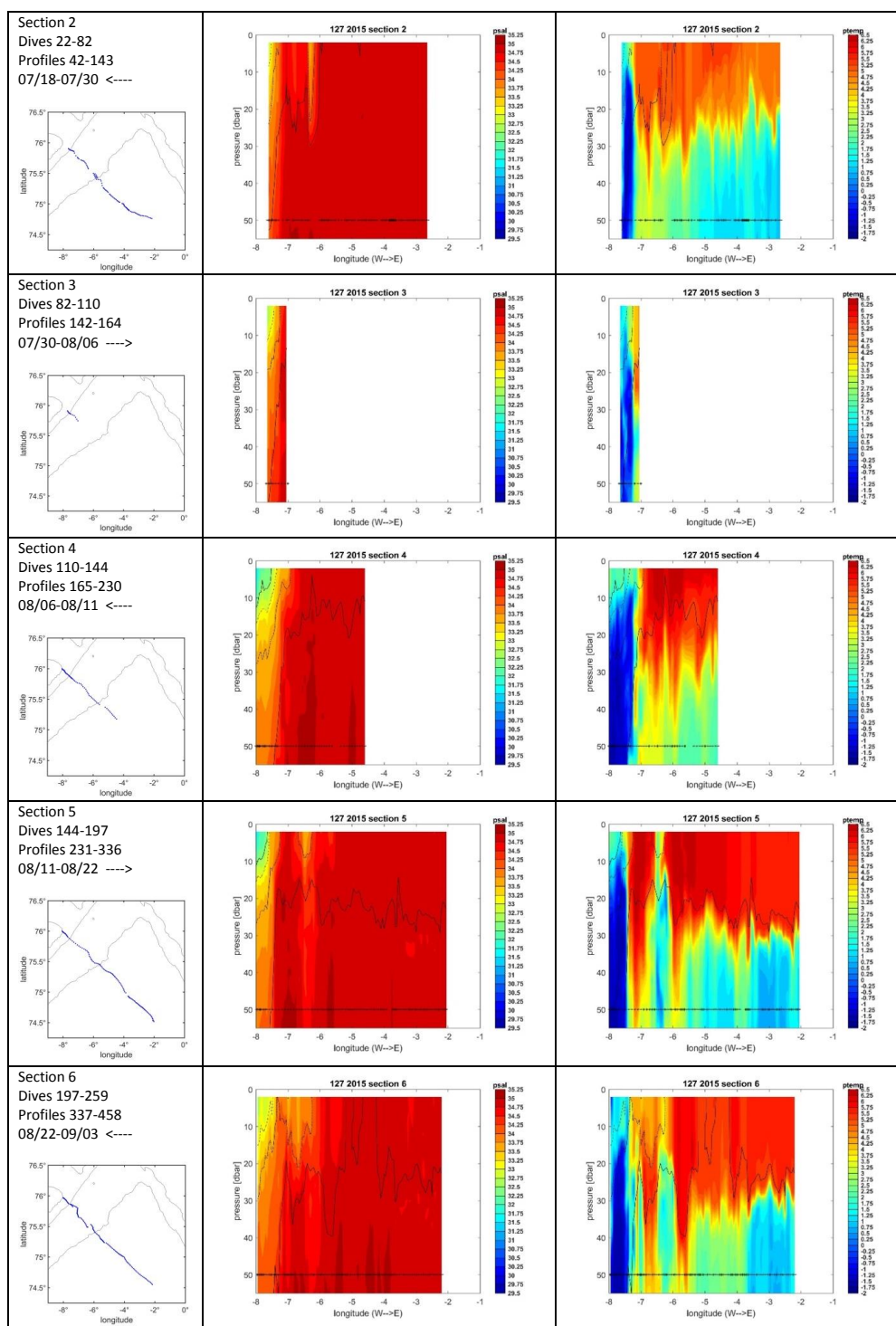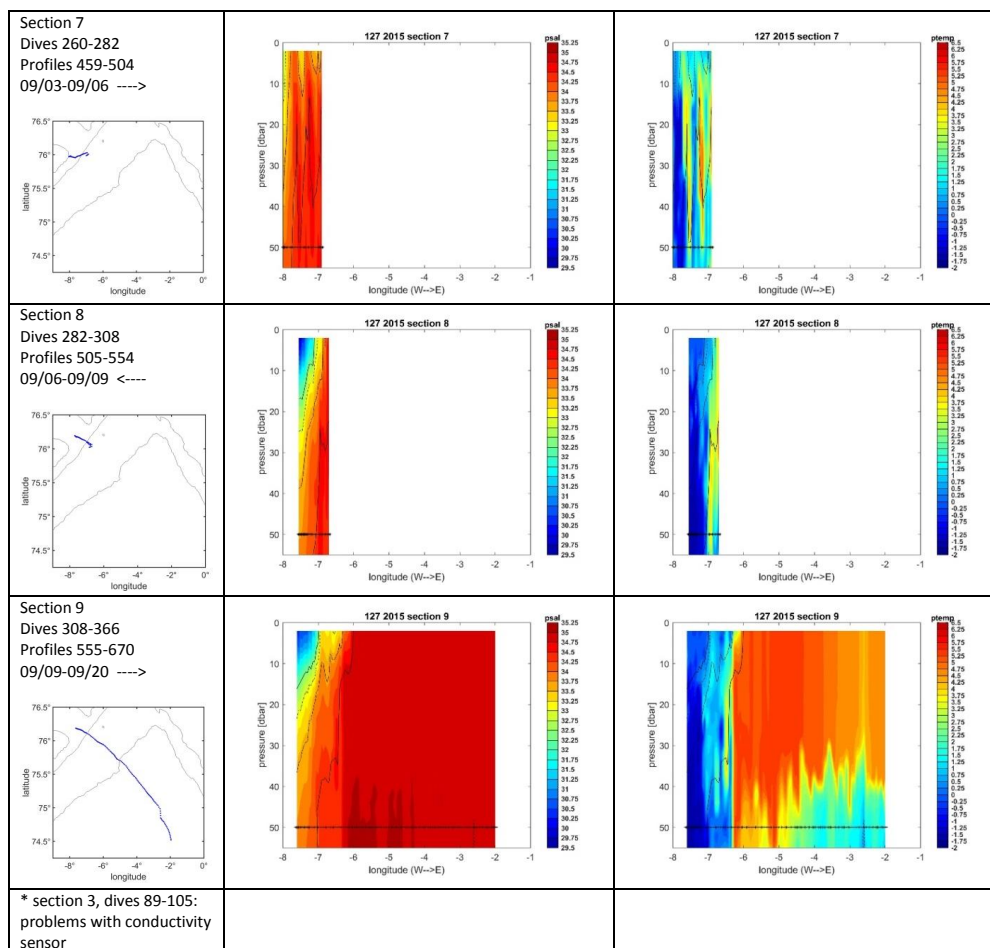
Figure 10: Sections: 2015, glider 127, sections 1-9. Shown are the upper 55m of the water column.
Left column: information and map extract with location of the profiles (no ice was observed during the whole mission time in the map extract); number of original dives on the section, number of profiles from the final dataset on the section, time span, and direction of the section: <--- east to west, ---> west to east.
Middle/right column: salinity/ potential temperature. Both plots are overlaid with the sigma-contours 26.0, 26.5, 27.0, 27.5 and 28.0 (see legend for line style in Fig. 7). Stars at 50 m depth mark the position of the profiles on the section before the gridding of the data in the horizontal toke place. For section 3 many profiles are missing because of problems with the conductivity sensor.

Competing interests

530   The authors declare that they have no conflict of interest.

Acknowledgements

Katrin Latarius was funded by the German Research Association (DFG) within the framework of the Research

535   Group FOR1740: "A new approach toward improved estimates of Atlantic Ocean freshwater budgets and

transports as part of the global hydrological cycle".

We thank Bastian Queste from the University of East Anglia for developing and making public available the

UEA toolbox and supporting us in using it.

During the mission piloting we got prompt, detailed and friendly support from KONGSBERG Germany as well

540   as KONGSBERG USA.

The piloting was conducted by Gerd Rohardt, Andreas Wiesotzki and Katrin Latarius from AWI with special

support from Harald Rohr,OPTIMARE.

During the missions Thomas Krumpen and his colleagues from DRIFT&NOISE provided high resolution ice

information.

545   We like to thank captain and crew of RV POLARSTERN and MV ORTELIUS and the Company OCEANWIDE

EXPEDITION for glider deployment and recovery under rough sea conditions.

References

550

Aagaard, K. and Carmarck, E.C.: The role of sea ice and other fresh water in the Arctic circulation. Journal of

Geophysical Research, 94 (C10), 14,485-14,498; 1989.

Alvarez, A. : A numerical analysis of the performance of unpumped SBE 41 sensors at low flushing rates. Deep-

Sea Research Part I 135, 46-55, doi:10.1016/j.dsr.2018.03.012, 2018.

555   Arndt, Jokat, W., Dirschel, B., Myklebust, R., Dowdeswell, J. A., and Evans, J.: A new bathymetry of the

Northeast Greenland continental shelf: Constraints on glacial and other processes, Geochemistry,

Geophysics, Geosystems 16, 3733-3753, doi:10.1002/2015GC005931, 2015.

Bamber, J., van den Broeke, M., Ettema, J., Lenaerts, J., and Rígnot, E.:Recent large increase in freshwater

fluxes   from   Greenland   into   the   North   Atlantic,   Geophysical   Research   Letters,   39,

560   doi:10.1029/2012GL052552, 2012.

Blindheim, J. and Rey, F.: Water-mass formation and distribution in the Nordic Seas during the 1990s, ICES

Journal of Marine Science, 61, 846-863, 2004.

Budéus, G. and Ronski, S.: An integral view of the hydrographic development in the Greenland Sea over a

decade, Open Oceanography J 3, 9-40, 2009.

565   Budéus, G. and Schneider, W.: On the hydrography of the Northeast water Polynya. Journal of Geophysical

Research 100(C3), 4269–4286, doi:10.1029/94JC02349, 1995.

Comiso, J.C., and Hall, D.: Climate trends in the Arctic as observed from space, WIREs Climate Change, 5, 389-

409, doi:10.1002/wcc.277, 2014.

Comiso, J.C., Parkinson, C.L., Gersten, R., and Stock, L.: Accelerated decline I the Arctic sea ice cover, Geophysical Research Letters, 35, doi:10.1029/2007GL031972, 2008.

Comiso, J.C., Wadhams, P., Pedersen, L.T., and Gersten, R.A.: Seasonal and interannual variability of the Odden ice tongue and s study of environmental effects, Journal of Geophysical Research 106(C5), 9093-9116, doi:10.1029/2000JC000204, 2001.

Davis, R.E., Eriksen, C.C., Jones, C.P. (2003) Autonomous buoyancy-driven underwater gliders. In: Technology and Applications of Autonomous Underwater Vehicles, ed. G. Griffiths, pp.37-58, London: Taylor & Francis

De Steur, L., R. S. Pickart, D. J. Torres and H. Valdimarsson (2015) Recent changes in the freshwater composition east of Greenland. GRL *42*, 2326–2332,

Dodd, P.A., Heywood, ., K.J., Meredith, ., M.P. , Naveira-Garabato, A.C., Marca, A.D., and Falkner, K.K. : Sources and fate of freshwater exported in the East Greenland Current, Geophysical Research Letters, 36, doi:10.1029/2009GL039663, 2009.

Frajka-Williams, E., Eriksen, C.E., Rhines, P.B., and Harcourt, R.R.: Determining Vertical Water Velocities from Seaglider, Journal of Atmospheric and Oceanic Technology, 28, doi:10.1175/2011JTECHO830.1, 2011.

Garau, B., Ruiz, S., Zhang, W.G., Pascual, A., Heslop, E., Kerfoot, J., and Tintore, J.: Thermal Lag Correction on Slocum CTD Glider Data, Journal of Atmospheric and Oceanic Technology, 28, 1065-1071, doi:10.1175/JTECH-D-10-05030.1, 2011.

Hansen, E., Gerland, S., Granskog, M.A., Pavlova, O., Renner, A.H.H., Haapala, J., Løyning, T.B., and Tschudi, M.: Thinning of the Arctic sea ice observed in Fram Strait: 1990-2011, Journal of Geophysical Research, doi:10.1002/jgrc.20393, 2013.

Hattermann, T., Isachsen, P.E., von Appen, W.-J., Albretsen, J., and Sundfjord, A.: Eddy-driven recirculation of Atlantic Water in Fram Strait, Geophysical Research Letters, 43, 3406-3414, doi:10.1002/2016GL068323, 2016.

Latarius,K. and Quadfasel, D. : Water mass transformation in the deep basins of the Nordic Seas: Analyses of heat and freshwater budgets, Deep-Sea Research I 114, 23-42, doi: 10-1016/j.dsr.2016.04.012, 2016.

Lherminier, P., Gascard, J.-C., and Quadfasel, D.: The Greenland Sea in Winter 1993 and 1994: preconditioning for deep convection. Deep-Sea Research, Part II 46, 1199-1235, 1999.

Lumpkin, R., and Speer, K.: Large-Scale Vertical and Horizontal Circulation in the North Atlantic Ocean, Journal of Physical Oceanography, 33, 1902-1920, 2003.

Morison, J., Andersen, R., Larson, N., D'Asaro, E., and Boyd, T.: The Correction for Thermal-Lag Effects in Sea-Bird CTD Data, Journal of Atmospheric and Oceanic Technology, 11, 1151-1164, 1994.

Nansen, F.: Northern waters. Captain Roald Amundsen's oceanographic observations in the Arctic Seas in 1901. Vidensk. Selsk. Skr. I. Mathematisk-Natur. Klasse, Christiania, j. Dybwad, 145 pp, 1906.

Oltmanns, M., Karstensen, J., and Fischer, J.: Increased risk of a shutdown of ocean convection posed by warm North Atlantic summers, Nature Climate Change, doi:10.1038/s41556-018-0105-1, 2018.

Quadfasel, D., Gascard, J.-C., and Koltermann, K.-P.: Large-Scale Oceanography in Fram Strait During the 1984 Marginal Ice Zone Experiment, Journal of Geophysical Research, 92(C7), 6719-6728, 1987.

Queste, B., Fernand, L., Juckells, T.D., Heywood, K.J., and Hind, A.J.: Drivers of summer oxygen depletion in the central North Sea, Biogeosciences, 13, 1209-1222, doi:10.5194/bg-13-1209-2016, 2016.

610   Rudels, B., Quadfasel, D., Friedrich, H., and Houssais, M.-N.: Greenland Sea convection in the winter of 1987-
            1988, Journal of Geophysical Research, 94(C3), 3223-3227, 1989.

       Rudels, B., Fahrbach, E., Meincke, J., Budéus, G., and Eriksson, P.: The East Greenland Current and its
            contribution to the Denmark Strait overflow. ICES Journal of Marine Science, 59, 1133-1154, 2002.

       Rudels, B., Björk, G., Nilsson, J., Winsor, D., Lake, I., and Nohr, C.: The Interaction between waters from the
615   Arctic Ocean and the Nordic Seas north of Fram Strait and along the East Greenland Current: results from
            the   Arctic   Ocean-O2   Oden   expedition.   Journal   of   Marine   Systems,   55,   1-30,   doi:
            10.1016/j.jmarsys.2004.06.008, 2005.

       Rudels, B., Korhonen, M., Budéus, G., Beszcynska-Möller, A., Schauer, U., Nummelin, A., Quadfasel, D., and
            Valdimarsson, H.: The East Greenland Current and its impacts on the Nordic Seas observed trends in the
620   past decade, ICES Journal of Marine Science, 69, 841-851, 2012.

       Rudnick, D.L., Davis, R.E., Erikson, C.C., Frantantoni D.M., Perry, M.J. (2004) Underwater gliders for ocean
            research. Mar. Technol. Soc. J. 38: 73-84.

       Schaffer, J., R. Timmermann, J. E. Arndt, S. S. Kristensen, C. Mayer, M. Morlighem, and D. Steinhage (2016),
            A global high-resolution data set of ice sheet topography, cavity geometry and ocean bathymetry, Earth
625   Syst. Sci. Data Discuss., 2016, 1–21, doi:10.5194/essd-2016-3.

       Schmitz, W.J., and McCartney, M.S.: On the North Atlantic circulation, Reviews of Geophysics, 31, 1, 29-49,
            1993.

       Schneider, W., and Budéus, G.: On the generation of the Northeast Water Polynya, Journal of Geophysical
            Research, 100(C3), 4269-4286, 1995.

630   Serreze, M.C. et al., 2006: The large.scale freshwater cycle of the Arctic. Journal of Geophysical Research,
            doi:10.1029/2005JC003424.

       Smedsrud, L.H., A. Sirevaag, K. Kloster, A. Sorteberg and S. Sandven, 2011: Recent wind driven high sea ice
            area export in the Fram Strait con tributes to Arctic sea ice decline. The Cryosphere,5, 821-829.

       Spall, M.:On the role of eddies und surface forcing in the heat transport and overturning circulation in marginal
635   seas, Journal of Climate, 24, 4844-4858, doi:10.1175/2011JCLI4130.1, 2011.

       Spreen, G., Kern, S., Stammer, D. and Hansen, E.: Fram Strait sea ice volume export estimated between 2003
            and 2008 from satellite data, Geophysical Research Letters, doi:10.1029/2009GL039591, 2009.

       Von Appen, W.-J., Schauer, U., Somavilla, R., Bauerfeind, E., and Beszczynska-Möller, A.: Exchange of
            warming deep waters across Fram Strait, Deep-Sea Research I 103, 86-100, 2015.

640